

Gamow-Teller transitions in magic nuclei calculated by the charge-exchange subtracted second random-phase approximation

M. J. Yang ¹, C. L. Bai ¹, H. Sagawa,^{2,3} and H. Q. Zhang⁴

¹*College of Physics, Sichuan University, Chendu 610065, China*

²*Center for Mathematics and Physics, University of Aizu, Aizu-Wakamatsu, Fukushima 965-8560, Japan*

³*RIKEN, Nishina Center, Wako 351-0198, Japan*

⁴*China Institute of Atomic Energy, Beijing 102413, China*



(Received 21 April 2022; accepted 7 July 2022; published 28 July 2022)

The Gamow-Teller (GT) transitions in four magic nuclei, ^{48}Ca , ^{90}Zr , ^{132}Sn , and ^{208}Pb , are studied using a self-consistent Hartree-Fock (HF) plus charge-exchange subtracted second random-phase approximation (SSRPA) model with several Skyrme energy density functions (EDFs). These calculations show that SSRPA improves systematically the description of main GT strength distributions in terms of the excitation energy and the peak height. The quenching factors are evaluated to be 13–20% of the Ikeda sum rule for ^{48}Ca , ^{90}Zr , and ^{132}Sn , due to the couplings to two-particle–two-hole (2p-2h) configurations. Also examined are the effects of tensor interactions on the excitation energies and the quenching factors of GT strength distributions.

DOI: [10.1103/PhysRevC.106.014319](https://doi.org/10.1103/PhysRevC.106.014319)

I. INTRODUCTION

Nuclear spin-isospin excitations are collective oscillations of a nucleus with spin and isospin degrees of freedom. They provide an unique opportunity to study the spin-isospin correlations in nuclei [1–3]. The GT excitation is the most well known spin-isospin mode with $J^\pi = 1^+$, and is closely linked to the electron capture and β decay rates. The GT excitation has a strong impact on the r -process nucleosynthesis together with the photonuclear cross sections [4]. In addition, the GT resonance is also associated with double- β decay processes, especially the two-neutrino double- β decay which take places through two GT-type transitions [5,6]. Microscopically, the GT transition is related to the spin-isospin component of the nucleon-nucleon interaction, and the precise description of the GT strength distribution is a significant mission for nuclear theories.

The theoretical studies of giant resonances in nuclei have made successful progress in the last two decades. Particularly, the microscopic models, such as the HF+(quasiparticle) random-phase approximation (RPA or QRPA) [7,8], which are based on the self-consistent mean-field approximation with the EDFs, have been largely developed over these years. The Skyrme EDFs [9–12] or Gogny [13–15] effective interactions are often adopted in these studies as well as the relativistic covariant effective Lagrangians [16–18]. Undoubtedly, (Q)RPA has achieved significant success in predicting the excitation energy of giant GT resonances with these effective Hamiltonians.

However, the (Q)RPA model including only one-particle–one-hole (1p-1h) configurations cannot provide a good account of the width of the giant resonance, such as the spreading width due to the coupling to the many-particle–

many-hole configurations [19–22]. Moreover, in the study of GT transitions, a large quenching of the sum rule value was found experimentally in the giant GT excitation energy region lower than 20 MeV [23].

In order to obtain a better description, models beyond the (Q)RPA approximation were proposed. The RPA plus particle-vibrations coupling (PVC) model was applied for charge-exchange excitations, in both nonrelativistic [24] and relativistic theoretical frameworks [25]. It was shown in Ref. [24] that the sum rule strength and the spreading width of GT state calculated by the PVC model are much better than the ones obtained by the RPA. Then, it was confirmed that the coupling with phonons can produce an appreciable quenching effect on the main GT resonances, but there are still some missing effects, such as the inclusion of tensor force and the coupling with high-energy 2p-2h configurations.

Very recently, the self-consistent HF+SSRPA model with Skyrme EDF, which takes into account the 2p-2h configurations reasonably, was applied to the GT transition in medium-light nucleus ^{48}Ca [26]. It was reported that the main GT strength distribution obtained by the SSRPA model shows a reasonable agreement with the experimental data in terms of the excitation energy. On top of that, the SSRPA model gives a quenching factor of about 25% due to the including of 2p-2h configurations. It was also reported in Ref. [27] that the SSRPA model incorporates the necessary correlations to provide an effective description of the quenching of GT spectra.

The spin-dependent excitations are in general affected by the tensor interactions more than the spin-independent ones [28]. The effect of the tensor force on the GT strength distribution of ^{90}Zr involved with 2p-2h coupling was reported in Ref. [29], which presented the result that the tensor force plays

an important role in shifting substantial amount of GT strength to a higher excitation energy region beyond the main GT resonance. Self-consistent HF+RPA calculations with tensor terms of Skyrme EDF were done in Refs. [30,31] for closed shell nuclei ^{90}Zr and ^{208}Pb . It was reported that the Skyrme-type tensor force shifts the GT main peaks downwards by about 2 MeV, and shifts about 10% of total GT strength to the high energy region.

In this work, self-consistent HF+SSRPA calculations based on the Skyrme EDFs are applied for the GT excitations of four closed shell nuclei, ^{48}Ca , ^{90}Zr , ^{132}Sn , and ^{208}Pb , to study the systematic trend of SSRPA for the description of GT strength distributions with respect to the excitation energy and the width. The effects of tensor force on the GT strength distribution and quenching problem will be also studied. The article is organized as follows. In Sec. II, a short summary of the formalism and some numerical details are presented. Results of the GT strength distributions calculated without the tensor force by RPA and SSRPA are shown for nuclei ^{48}Ca , ^{90}Zr , ^{132}Sn and ^{208}Pb in Sec. III. The effects of the tensor force on the GT strength distribution and the quenching in the HF+SSRPA model will be given in Sec. IV. A summary is given in Sec. V.

II. FORMALISM AND NUMERICAL DETAILS

The operator for GT transitions is defined as

$$\hat{O}_{GT\pm} = \sum_{i=1}^A \sigma(i)t_{\pm}(i), \quad (1)$$

where σ is the spin operator and $t_{\pm} = t_x \pm it_y$ are the isospin raising and lowering operators, respectively. The total GT strength obeys the model independent Ikeda sum rule [32],

$$S_- - S_+ = 3(N - Z). \quad (2)$$

The present research is focused on the GT_- strength distributions, owing to the fact that the GT_+ transition is suppressed in nuclei with a significant neutron excess.

The quenching factor for the transition strength in our discussion is defined as

$$Q = \frac{3(N - Z) - \sum_{0 < E_x < E_{\max}} B(GT : E_x)_{\text{calc}}}{3(N - Z)}. \quad (3)$$

As the charge-exchange SRPA and SSRPA models are well described in Refs. [21,33], we give only few necessary formulation about our numerical implementation. We start by solving the HF equations in coordinate space with a radial mesh extending up to 20 fm in a step of 0.1 fm. When the Skyrme HF potential is calculated, the single-particle energies and wave functions of the occupied and unoccupied levels can be solved by using the harmonic oscillator basis. This basis is large enough to ensure that our results are stable. For the truncation of configurations, the energy cutoff on the 1p-1h configurations is set as 100 MeV. For the 2p-2h configurations, to make the problem tractable, the truncations of 2p-2h configurations are set as 40 MeV for ^{48}Ca and ^{90}Zr , 30 MeV for ^{132}Sn . It has been checked that the results do

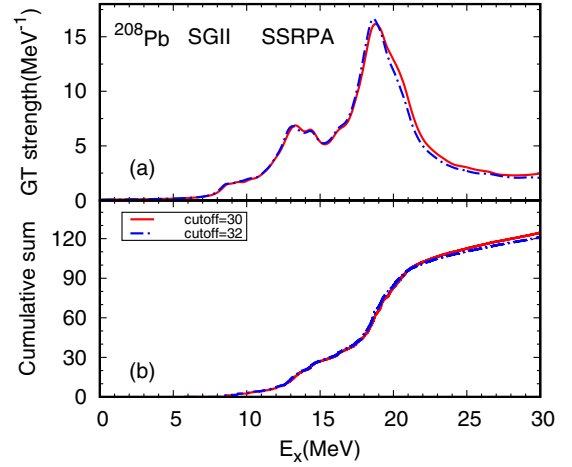


FIG. 1. The strength distributions and corresponding cumulative sums of ^{208}Pb calculated by SSRPA with SGII for 2p-2h energy cutoffs of 30 and 32 MeV. The red line represents cutoff = 30 MeV and the blue dashed line represents cutoff = 32 MeV.

not change significantly when the cutoff is raised beyond that level. In addition, the cutoff for ^{208}Pb is set as 30 MeV, due to the huge configuration number. The cutoff 32 MeV is also tested for ^{208}Pb , and the results are shown in Fig. 1. In this work, the discrete GT strength distributions are smoothed with a Lorentzian weighting function having 1 MeV width. As shown in the figure, the excitation energy of the giant resonance is changed within 0.1 MeV due to the change of the cutoff from 30 to 32 MeV, and the cumulative sums are almost the same below $E_x = 25$ MeV, but the quenching factor is enlarged by about 3% in the case of $E_{\max} = 32$ MeV. Therefore, we will hereafter mainly discuss the strength distributions of ^{208}Pb below $E_x = 25$ MeV. For the quenching in ^{208}Pb , it looks insufficient to set the cutoff even at 32 MeV, but a higher cutoff will be beyond our computing power, so the present results are of value for the description of giant GT resonance.

We performed two SSRPA calculations in the four nuclei with SGII EDF: one is the full calculation without further approximation, and another is the diagonal approximation of the coupling matrix elements A_{22} between 2p-2h configurations applied only in the subtracted procedure. It has been confirmed that the result obtained with the diagonal approximation used in the subtraction procedure is almost the same as the one produced by the full calculation for medium-heavy nuclei. For a simple example, Fig. 2 shows the results of the full calculation and the one obtained with the diagonal approximation in the subtraction procedure for ^{90}Zr . The figure shows that the strength distributions of the two calculations differ only less than 0.1 MeV in the excitation energy, and the quenching factors are kept unchanged, which is consistent with what was reported in Ref. [27]. Therefore, hereafter, the diagonal approximation of A_{22} is adopted in the subtraction procedure for ^{90}Zr , ^{132}Sn , and ^{208}Pb , and the full calculations are always performed for ^{48}Ca . More details about our SSRPA calculations can be found in Ref. [34].

In the present calculations, Skyrme EDFs SGII [35], SAMi [36], SAMi-T [37], and several ones from the TIJ family

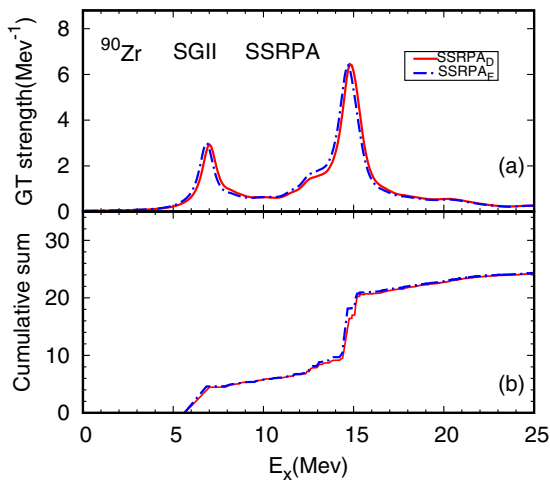


FIG. 2. The strength distributions and corresponding cumulative sums of ^{90}Zr calculated by SSRPA with SGII for the full calculation and the diagonal approximation used in the subtraction procedure one. The red line represent the result obtained with the diagonal approximation used in the subtraction procedure, labeled SSRPA_D , and the blue dashed line represents the full calculation, labeled SSRPA_F .

[38] are employed. The SGII and SAMi-T EDFs are able to well reproduce the excitation energies of the GT resonances in magic nuclei in RPA or RPA+PVC calculations [24,39], which means better spin-isospin characters of the nucleon-nucleon interaction in these EDFs. In order to study in a sense simply the effects of tensor force with different strengths but the central part kept unchanged, the SGII+Te1, SGII+Te2, and SGII+Te3 EDFs are also applied in the calculations, which take into account the excitation energies of the GT and charge-exchange spin-dipole resonances in ^{90}Zr and ^{208}Pb through the HF+RPA calculations [40]. Since one of the main motivations of this work is the effect of tensor interactions, which contribute to the EDF in terms of J^2 , the J^2 terms are included in both HF and residual interaction in order to keep consistency in all the calculations. In addition, as the SGII EDF was fitted without J^2 terms, we also will perform the calculations in which J^2 terms from the central part of the interaction (the momentum dependent terms of Skyrme EDF) are excluded in both HF and residual interactions for SGII, but the tensor terms are included in J^2 terms. The results will be discussed at the last part of Sec. IV.

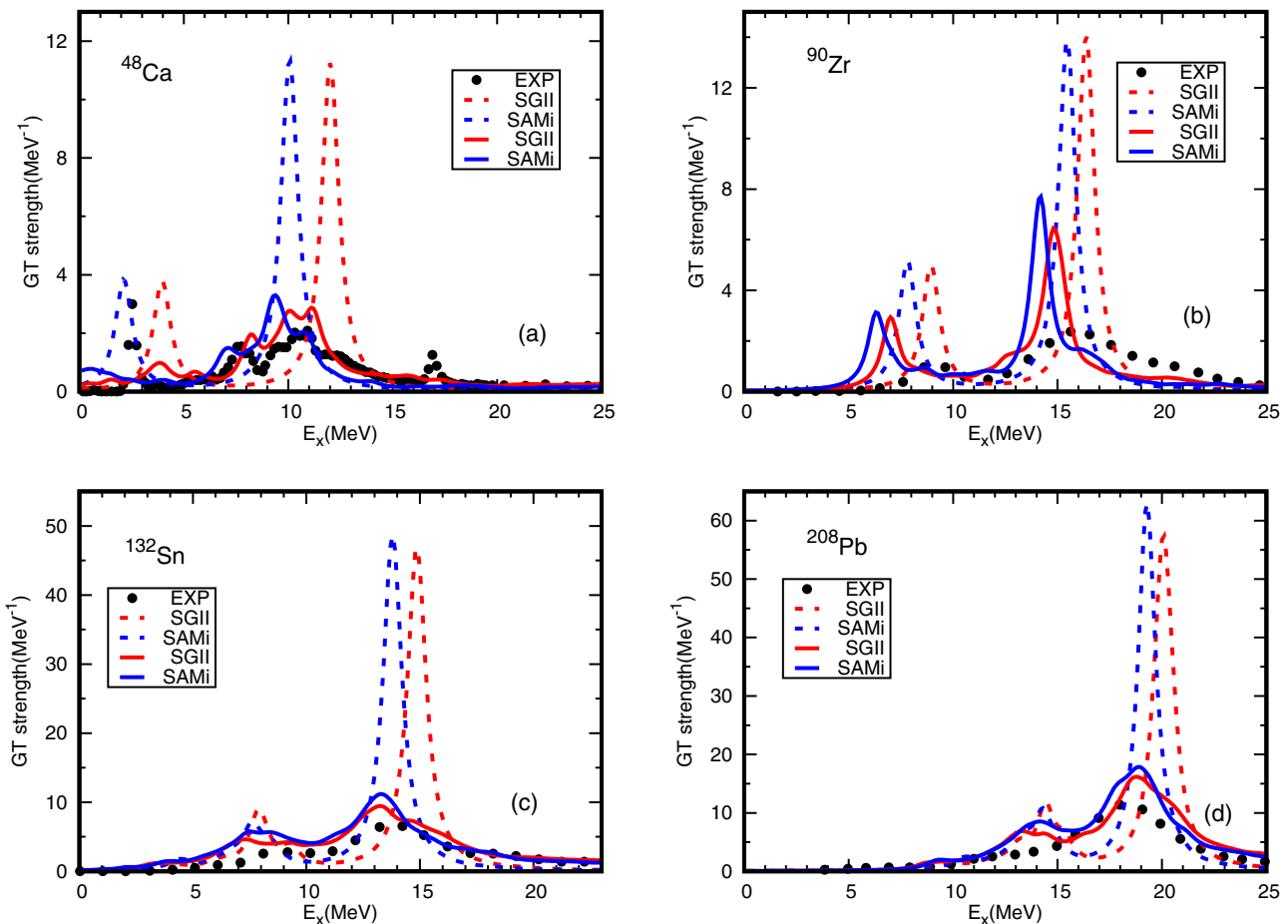


FIG. 3. GT strength distributions of ^{48}Ca [panel (a)], ^{90}Zr [panel (b)], ^{132}Sn [panel (c)], and ^{208}Pb [panel (d)] calculated with the SGII and SAMi EDFs by RPA (dashed lines) and SSRPA (solid lines). The results obtained by SGII and SAMi are shown by the red and blue lines, respectively. The experimental data of ^{48}Ca [41], ^{90}Zr [42], ^{132}Sn [43], and ^{208}Pb [44] are shown by the black filled circles. The calculated discrete strength distributions are smoothed by a Lorentzian weighting function of 1 MeV width. See the text for more details.

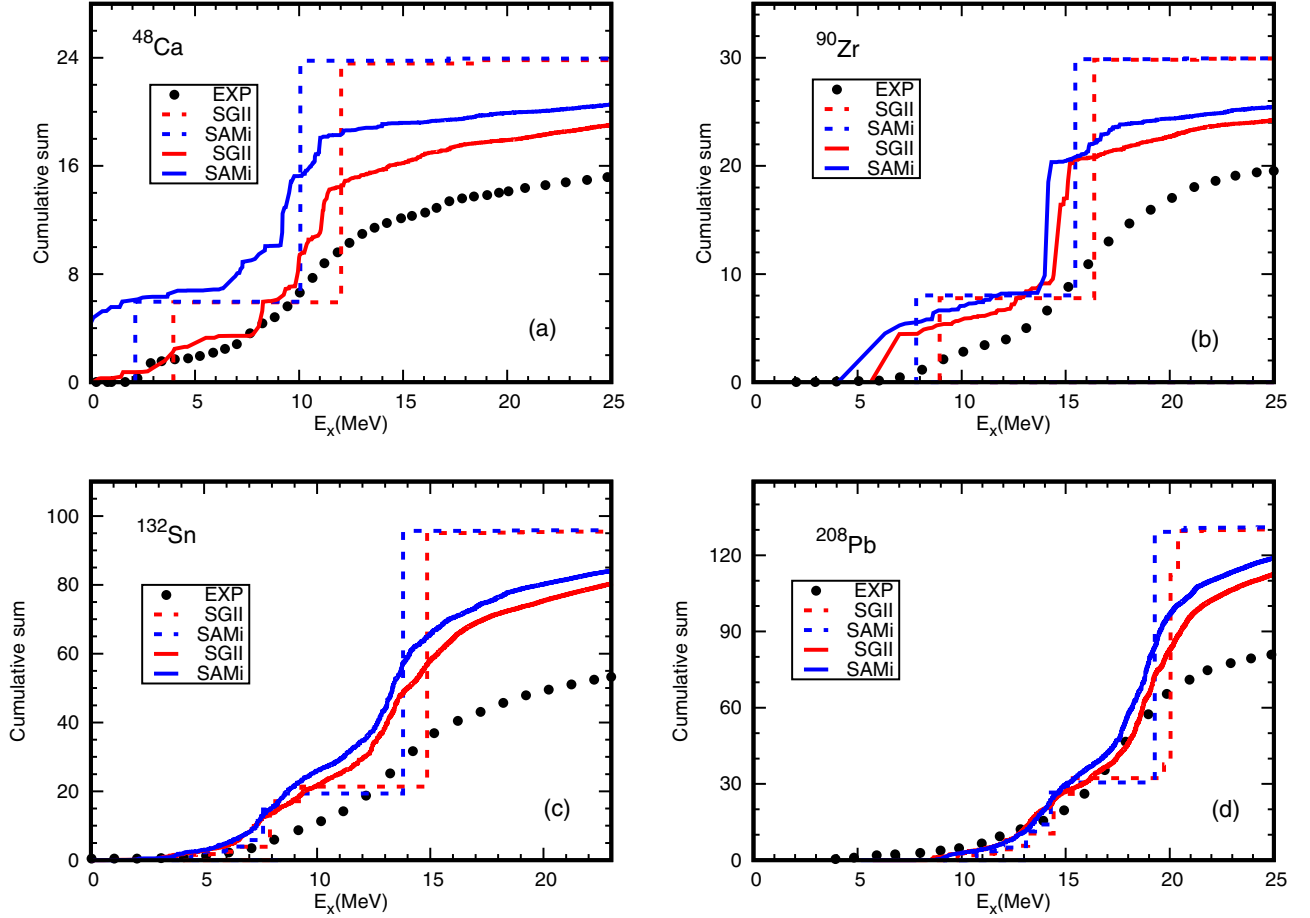


FIG. 4. Cumulative GT_- strengths up to 25 MeV for ^{48}Ca [panel (a)] and ^{90}Zr [panel (b)], 23 MeV for ^{132}Sn [panel (c)], and 25 MeV for ^{208}Pb [panel (d)] calculated with SGII and SAMi by RPA (dashed lines) and SSRPA (solid lines). The results obtained by SGII and SAMi are shown by the red and blue lines, respectively. The experimental data of ^{48}Ca [41], ^{90}Zr [42], ^{132}Sn [43], and ^{208}Pb [44] are shown by the black filled circles.

III. SPREADING OF GT STATES IN SSRPA

Figure 3 shows the strength distributions of ^{48}Ca [panel (a)], ^{90}Zr [panel (b)], ^{132}Sn [panel (c)], and ^{208}Pb [panel (d)] calculated with SGII (red lines) and SAMi (blue lines) by RPA (dashed lines) and SSRPA (solid lines), together with the experimental data. As shown in the figure, in RPA calculations, the excitation energies of the main peaks are well reproduced by SAMi, and SGII gives the main peak about 1–2 MeV higher than that of SAMi. Moreover, RPA obtain strengths in the main peaks much larger than the experimental ones by a factor of 5 to 7, which is the typical defect of the RPA model. In the results calculated by SSRPA, quantitative improvements for the description of GT strength distribution are observable. One can observe that the strengths in the main peaks are expanded in a wide energy region due to the spreading effect of the 2p-2h coupling. As a result, the strengths of the main peaks are about 1.5 times those of the experimental ones in ^{48}Ca , ^{132}Sn , and ^{208}Pb , and about 3–4 times those in ^{90}Zr . Moreover, in the SSRPA model, the main peak may be shifted downwards. When calculated with SGII, the main peaks are shifted downward by about 1 to 1.5 MeV in the four nuclei, which well reproduces the experimental

data, while in the case of SAMi the main peaks are shifted downwards by about 1 and 1.5 MeV respectively in ^{48}Ca and ^{90}Zr but are almost kept unchanged in ^{132}Sn and ^{208}Pb . The corresponding cumulative sums are shown in Fig. 4. The results calculated with SGII and SAMi are labeled by red and blue lines, respectively. As extracted from the figure, the experimental quenching factors are about 36.7%, and 34.9% with $E_{\text{max}} = 25$ MeV, respectively, for ^{48}Ca and ^{90}Zr , 44.5% for ^{132}Sn with $E_{\text{max}} = 23$ MeV, and 38.6% for ^{208}Pb with $E_{\text{max}} = 25$ MeV. These maximum energies are selected by the limit of available experimental data of each nucleus without large uncertainty. One can see that the cumulative sums obtained by the RPA model evolved very steeply at the main peak energy regions, and reach the sum rule limit. In the SSRPA model, the cumulative sums increase gradually, and the quenching factors obtained with SGII (SAMi) are respectively about 20.7% (14.4%) for ^{48}Ca , 19.2% (15.2%) for ^{90}Zr , 16.4% (12.5%) for ^{132}Sn , and 14.7% (10.0%) for ^{208}Pb in the energy region corresponding to the experimental results. For these nuclei, the SGII EDF gives about 5% larger quenching than that of SAMi. About a half of the experimental quenching factor is obtained by the calculated results of SSRPA with SGII for ^{48}Ca and ^{90}Zr , and about 40% for ^{132}Sn and ^{208}Pb .

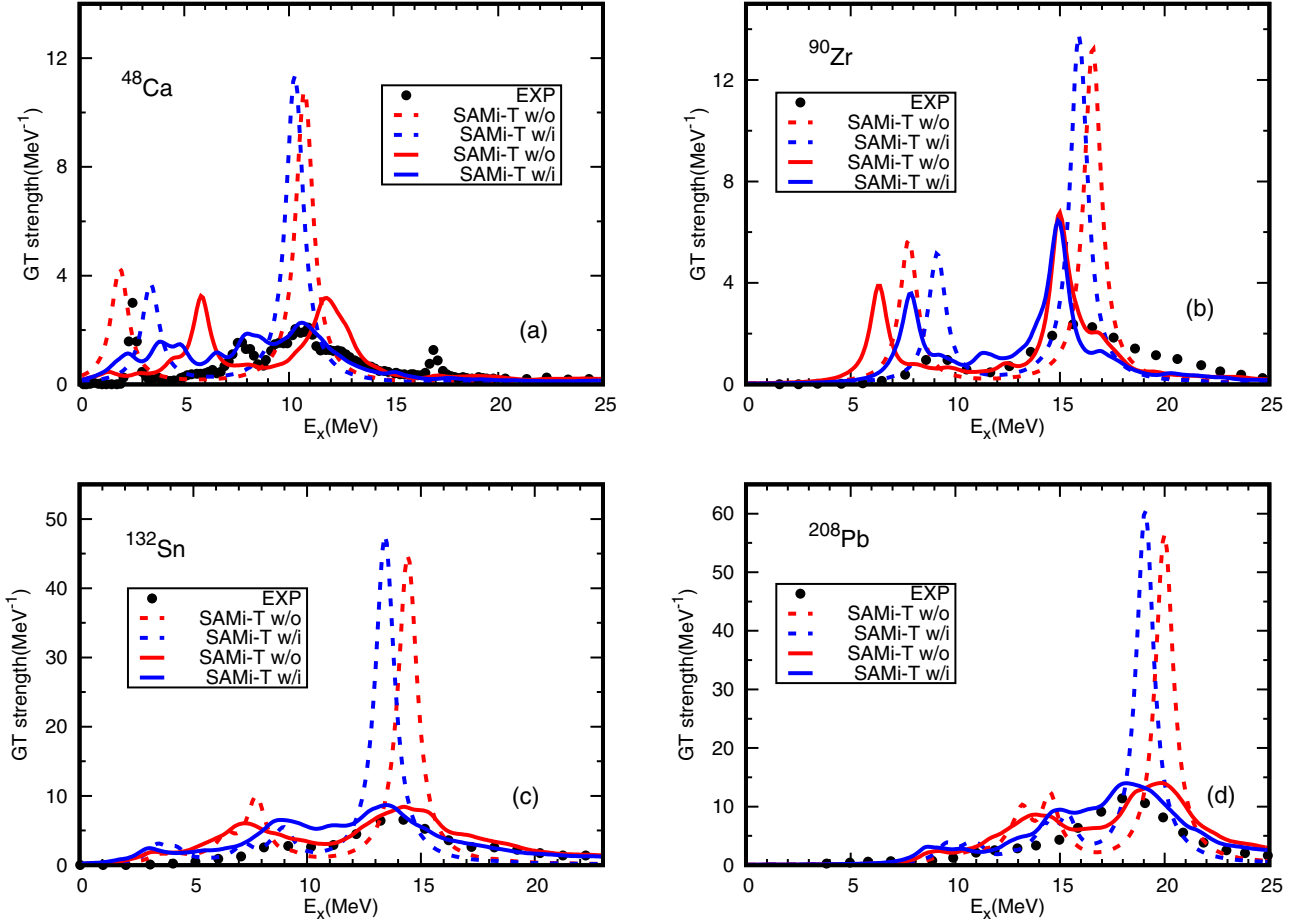


FIG. 5. The same as Fig 3, but for the SAMi-T EDF with or without tensor terms. Red lines represent SAMi-T without tensor terms, labeled w/o, and blue lines represent the SAMi-T EDF with tensor terms, labeled w/i.

The quenching factor might be further changed by the tensor force [29]. We will study this point in the next section.

In the SSRPA calculation with SGII and SAMi, the spreading effects on the GT strength produce the shape of giant GT resonances close to the experimental ones. The giant resonances might be shifted downward by about 1 to 1.5 MeV due to the 2p-2h coupling in SSRPA. As a result, the GT strength distributions of the four nuclei can be well described by the present SSRPA model, particularly with the SGII EDF.

IV. EFFECTS OF TENSOR FORCE

As was reported in the literatures [30,31,39], the tensor correlations in the RPA model have strong influence on GT resonances. In this section, we discuss the effect of tensor terms of the Skyrme EDF in the SSRPA model. As the strength of the tensor force of Skyrme EDF is not well optimized for the spin-isospin excitations, we do the calculation first with the Skyrme EDFs whose parameters are optimized with tensor terms to reproduce a set of experimental observables, i.e., SAMi-T and three other ones from TIJ family. It should be noticed that one of the ingredients of optimization procedure of the SAMi-T EDF is the Landau-Migdal parameter for the spin-isospin channel. Second, in order to

find a particular role of tensor force on the GT states, we select different choices of tensor terms on top of the existing Skyrme EDF parameters. To this end, we do the calculations with SGII+Te1, Te2, and Te3, in which the central part of the EDF is kept unchanged and the tensor forces are varied in an acceptable region to describe well the GT and spin-dipole excitations, as far as the excitation energies of main peaks in several nuclei are concerned [40]. In the end of this subsection, the effects of J^2 terms originating from the momentum dependent terms of the Skyrme EDF will be discussed, since both the momentum dependent terms and the tensor force make contributions to the J^2 terms of EDF.

Figure 5 shows the strength distributions calculated with the SAMi-T EDF with and without tensor terms in RPA and SSRPA models. The red and blue lines represent the calculations without and with tensor force, respectively. As shown in this figure, in RPA calculations without the tensor force, the excitation energies of the main peaks appear about 1–2 MeV higher in energy than those with the tensor force in all nuclei. In SSRPA calculations, the tensor force shifts the main peaks downwards by about 1 to 1.5 MeV and the peak heights are reduced to be almost the same as the experimental ones in ^{48}Ca , ^{132}Sn , and ^{208}Pb . Particularly, in ^{48}Ca , the inclusion of the tensor terms reproduces well not

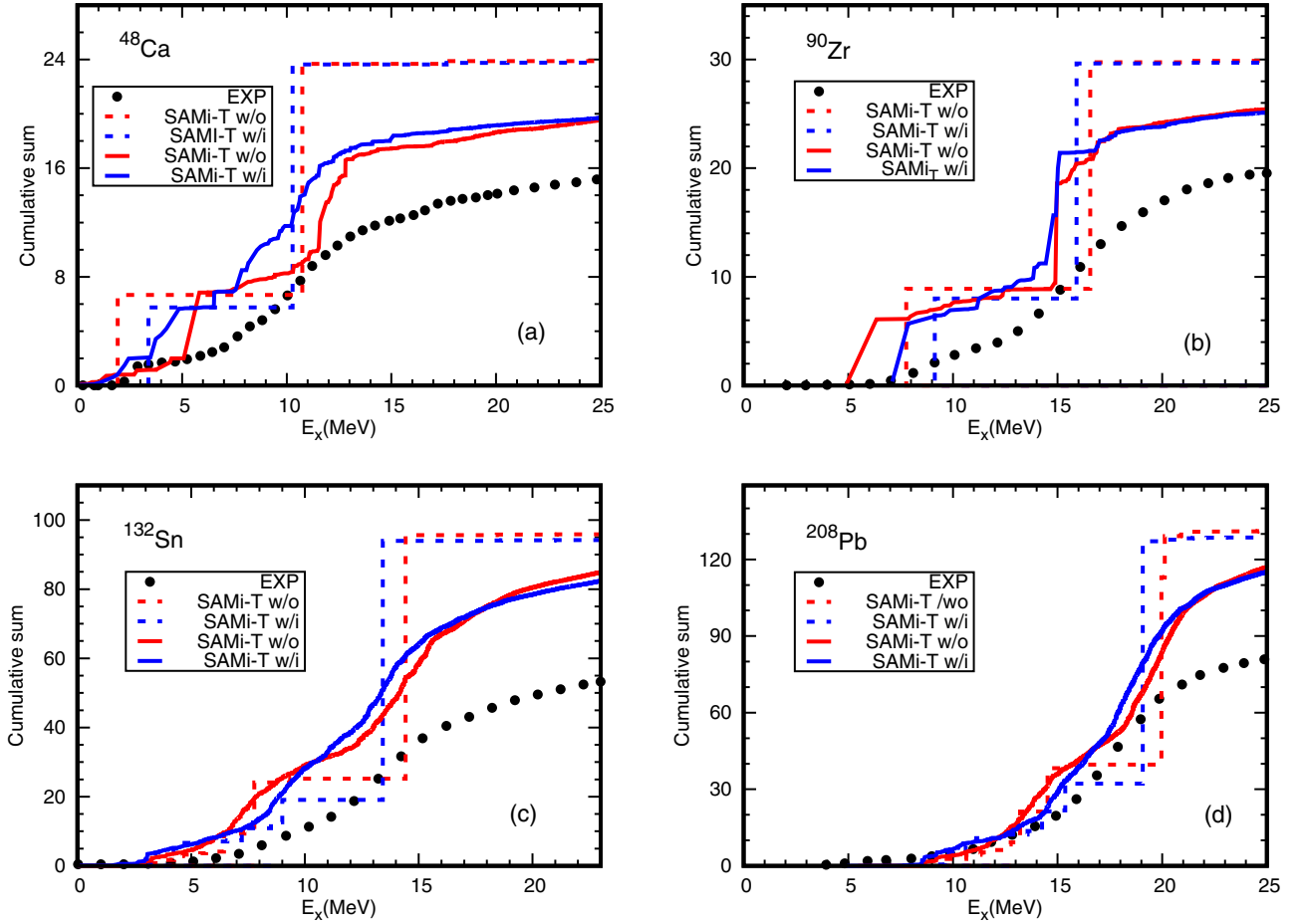


FIG. 6. The same as Fig 4, but for the SAMi-T EDF with or without tensor terms. Red lines represent SAMi-T without tensor terms, labeled w/o, blue lines represent SAMi-T with tensor terms, labeled w/i.

only the main peak at $E_x = 11$ MeV, but also the shoulder at around $E_x = 7.5$ MeV. We can see also better descriptions of main peaks in ^{132}Sn and ^{208}Pb in terms of the excitation energy and the peak heights. On the other hand, in ^{90}Zr , the excitation energy of the main peak is almost unchanged by the tensor force, and the agreement with the experimental data is modest.

The corresponding cumulative sums are shown in Fig. 6. The gross feature of RPA and SSRPA calculations is similar to that of SAMi shown in Fig. 4, i.e., the SSRPA calculations show gradual increase of the sum until $E_x = 15$ MeV, showing a trend similar to the experimental ones, while those of RPA show abrupt increase at the main GT peak energies. The quenching factors obtained by the SSRPA model give just few-percent changes after including tensor terms. This might be due to the weak strength of the tensor force in SAMi-T. In order to explore the effect of tensor terms with different strengths on the quenching problem, T21, T44, and T55 EDFs from the TIJ family are adopted in the SSRPA calculations. The strength distributions and corresponding cumulative sums of ^{48}Ca , ^{90}Zr , ^{132}Sn , and ^{208}Pb calculated with T21, T44, and T55 by SSRPA are shown in Fig. 7. In general, the TIJ family give poor results for the descriptions of GT states since the spin-isospin excitations are not included in the optimization procedure of the EDF parameters. Nevertheless, these param-

eter sets might be useful to explore how different strengths of tensor terms affect the properties of GT strength distributions.

In ^{48}Ca , T21 and T55 EDFs give main peaks lower in energy by 10 and 3 MeV, respectively, compared with the experimental peak, while T44 EDF successfully produces the main peak. In ^{90}Zr , T44 and T55 EDFs give acceptable results for the main peak, slightly underestimating the excitation energy by about 1 MeV, but these EDFs show a low energy peak at around $E_x = 5$ MeV with strength comparable to the main peak, which is quite different from the experimental data. For ^{132}Sn and ^{208}Pb , all of the three EDFs fail to describe the strength distributions.

The quenching factors of the four nuclei calculated by the three EDFs, as well as the corresponding strength of the tensor force are listed in Table. I. As shown in the table, the strength of triplet-even tensor term T in the three EDFs is around 500 MeV fm^5 , while the strength of the triplet-odd tensor term U is quite different even in the sign. One can notice that, for T55 with positive U , the quenching factors are large: about 30% in ^{48}Ca , 25% in ^{90}Zr , 27% in ^{132}Sn , and 19% in ^{208}Pb . For ^{208}Pb , the quenching factors are smaller in Table. I, which might be related to the insufficient energy cutoff, as was discussed in Sec. II. These results indicate that the tensor term U with the certain strength has a stronger effect on the quenching. For TIJ family, the tensor terms are changed

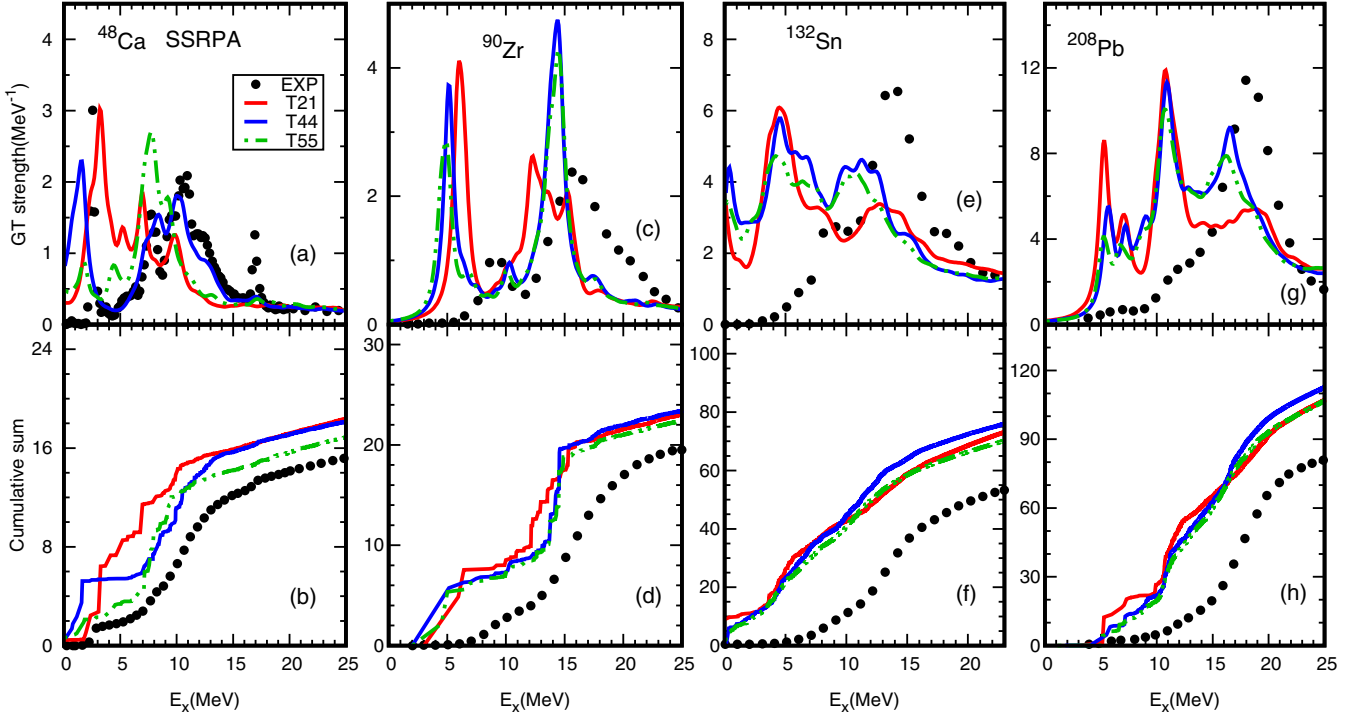


FIG. 7. Strength distributions (upper panels) and corresponding cumulative sums (lower panels) of ^{48}Ca [panels (a), (b)], ^{90}Zr [panels (c), (d)], ^{132}Sn [panels (e), (f)], and ^{208}Pb [panels (g), (h)] calculated with the T21, T44, and T55 EDFs by SSRPA. The results obtained by T21, T44, and T55 are labeled by red solid lines, blue solid lines, and green dash-dot-dot lines, respectively. The experimental data are shown by the black filled circles.

and the central terms of Skyrme EDFs are also changed. Therefore, we further pursue the effect of tensor force to change the strength of the tensor terms, keeping the central part unchanged.

The role of the Skyrme tensor terms in the RPA calculations of Gamow-Teller and spin-dipole states, varying the signs and magnitude of tensor terms, was discussed extensively in the literature [40], in which different strengths of the tensor force are added on top of the same SGII EDF. We employ three parameter sets, SGII+Te1, SGII+Te2, and SGII+Te3, whose tensor parameters are listed in Table II, which give reasonable descriptions of GT and spin-dipole excitations.

The strength distributions and corresponding cumulative sums of ^{48}Ca , ^{90}Zr , ^{132}Sn , and ^{208}Pb calculated with SGII,

SGII+Te1, SGII+Te2, and SGII+Te3 by the SSRPA model are shown in Fig. 8. As shown in this Figure, the SGII+Te1 EDF reduces the peak height of the main GT peak, but the excitation energy is not much changed compared with the results of SGII. Thus the SGII+Te1 EDF reproduces well the main GT peaks in ^{48}Ca , ^{132}Sn , and ^{208}Pb in terms of both the excitation energy and the peak height, but underestimates the energy by about 1.5 MeV in ^{90}Zr . The SGII+Te2 EDF gives a good account of the main peak energy in ^{48}Ca , but underestimates the peak energies by about 2.5 MeV in ^{90}Zr , ^{132}Sn , and by about 1 MeV in ^{208}Pb . The peak heights of the main GT

TABLE II. The same as Table I, but calculated with SAMi, SAMi-T, SGII, SGII+Te1, SGII+Te2, SGII+Te3, SGII⁰, SGII⁰+Te1, SGII⁰+Te2, and SGII⁰+Te3 EDFs.

TABLE I. The quenching factor calculated by SSRPA with the T21, T44, and T55 EDFs. The strengths of tensor terms are also given. The cumulative sums are taken up to $E_{\text{max}} = 25$ MeV for ^{48}Ca and ^{90}Zr , 23 MeV for ^{132}Sn , and 25 MeV for ^{208}Pb , consistent with those of Fig. 7.

Force	(T, U)	^{48}Ca	^{90}Zr	^{132}Sn	^{208}Pb
T21	(476.9, -369.4)	23.6%	23.3%	23.8%	18.9%
T44	(521.0, 21.5)	24.5%	22.0%	20.8%	14.6%
T55	(564.6, 129.3)	29.7%	25.3%	26.9%	19.1%
Expt.		36.7%	34.9%	44.5%	38.6%

Force	(T, U)	^{48}Ca	^{90}Zr	^{132}Sn	^{208}Pb
SAMi	(0,0)	14.4%	15.2%	12.5%	10.0%
SAMi-T	(415.5, -95.5)	18.6%	16.3%	14.2%	12.7%
SGII	(0,0)	20.7%	19.2%	16.4%	14.7%
SGII+Te1	(500, -350)	28.7%	26.6%	28.7%	27.3%
SGII+Te2	(600, 0)	23.8%	22.1%	23.3%	19.0%
SGII+Te3	(650, 200)	22.9%	24.1%	27.6%	23.6%
SGII ⁰	(0,0)	34.4%	29.4%	31.4%	33.2%
SGII ⁰ +Te1	(500, -350)	39.8%	35.0%	42.8%	43.2%
SGII ⁰ +Te2	(600, 0)	37.9%	31.0%	35.8%	31.7%
SGII ⁰ +Te3	(650, 200)	34.8%	32.6%	40.6%	35.0%
Expt.		36.7%	34.9%	44.5%	38.6%

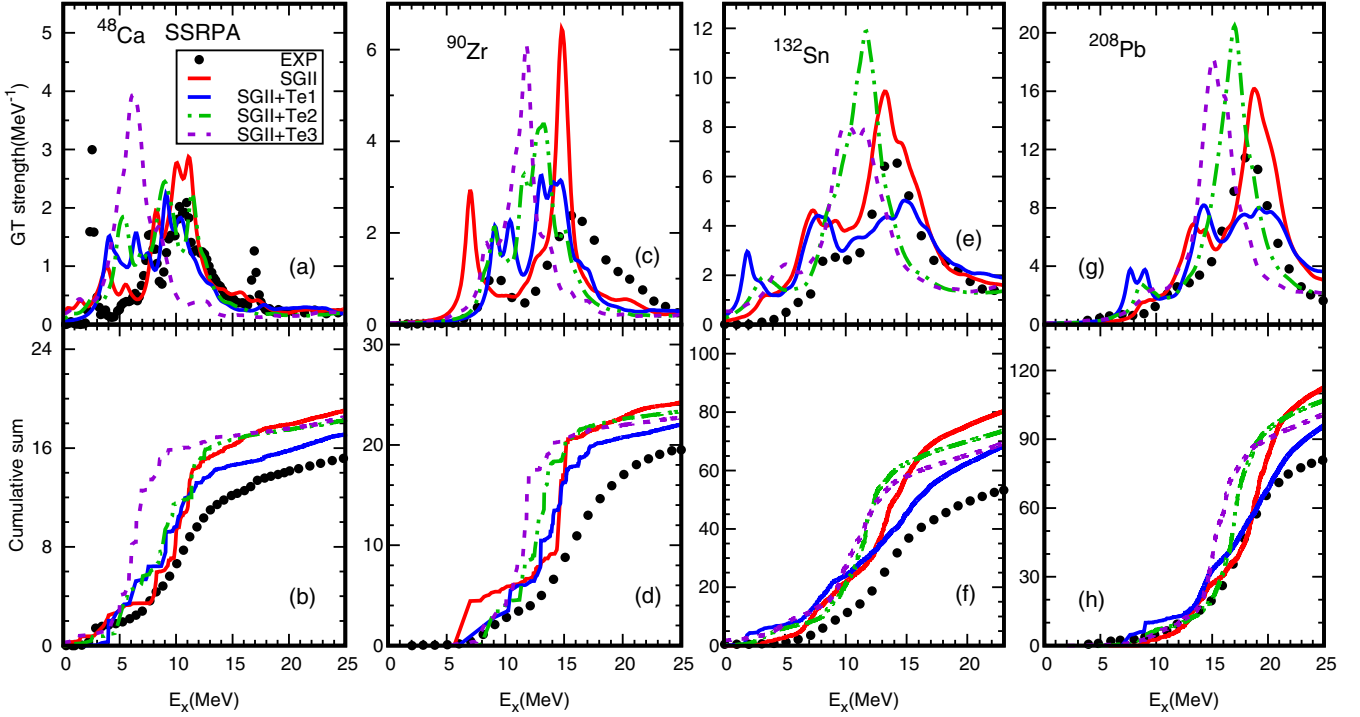


FIG. 8. Strength distributions (upper panels) and corresponding cumulative sums (lower panels) of ^{48}Ca [panels (a), (b)], ^{90}Zr [panels (c), (d)], ^{132}Sn [panels (e), (f)], and ^{208}Pb [panels (g), (h)] calculated with the SGII, SGII+Te1, SGII+Te2, and SGII+Te3 EDFs by SSRPA. The results obtained by SGII, SGII+Te1, SGII+Te2, and SGII+Te3 are shown by red solid lines, blue solid lines, green dash-dot-dot lines, and violet dashed lines, respectively. The experimental data are shown by the black filled circles.

peaks are overestimated by the SGII+Te2 in ^{90}Zr , ^{132}Sn , and ^{208}Pb . The SGII+Te3 EDF is poorer than the other two EDFs, underestimating the excitation energies by about 5 MeV in ^{48}Ca and ^{90}Zr and by about 3 MeV in ^{132}Sn and ^{208}Pb . For the widths of the main peaks, the SGII+Te1 EDF gives strong effects in the four nuclei, i.e., the strengths are distributed in wide energy regions and the main peaks are fragmented, while the SGII+Te2 EDF gives some fragmentations of the main GT peaks in ^{48}Ca and ^{90}Zr , but merges the strengths to one peak in ^{132}Sn and ^{208}Pb . The SGII+Te3 EDF has no effect of making larger widths of the main peaks compared with the SGII EDF without the tensor terms.

The quenching factors for the four nuclei ^{48}Ca , ^{90}Zr , ^{132}Sn , and ^{208}Pb together with the strengths of tensor forces of SAMi, SAMi-T, SGII, SGII+Te1, SGII+Te2, and SGII+Te3 are listed in Table II. In general, the tensor interactions give more quenching than those without the tensor force. One interesting point to observe from the table is that the SGII+Te1 and SGII+Te3 with the triplet-odd tensor U term give more quenching than the one without the U term, which is consistent with the results of the TIJ family. Especially, the quenching factors calculated with the SGII+Te1 EDF are systematically increased by about 10% in comparison with the SGII EDF in the four nuclei. This indicates that the tensor forces with stronger strengths give larger quenching factors, being close to the experimental data, and are consistent with the calculated results in Ref. [29].

In the above calculations the J^2 terms are included in both HF and SSRPA, but in the original SGII they were

not included in the HF level. For this reason, we perform calculations in which the J^2 terms from the momentum dependent part of the Skyrme interactions are excluded in both HF and SSRPA for SGII. The results are labeled by SGII⁰ in order to distinguish from the ones with J^2 terms. Figure 9 shows the strength distributions and corresponding cumulative sums of ^{48}Ca , ^{90}Zr , ^{132}Sn , and ^{208}Pb calculated with SGII⁰, SGII⁰+Te1, SGII⁰+Te2, and SGII⁰+Te3. Compared with the results with all the J^2 terms, those in Fig. 9 reduce substantially the strengths of main peaks in all nuclei, as can be seen also in the quenching factors in Table II. The results of SGII⁰ irrespective to the tensor interactions give additional 10–20 % quenching in Table II. In the strength distributions, the SGII⁰ EDF without tensor terms reproduces well the main peaks of ^{48}Ca and ^{90}Zr , but results are not so good for those of ^{132}Sn and ^{208}Pb . On the other hand, SGII⁰+Te2 and SGII⁰+Te3 give good accounts of main peaks of ^{132}Sn and ^{208}Pb , but underestimate the peak energy of ^{90}Zr . Thus, SGII⁰ EDFs have an advantage to give a large quenching factor, especially the SGII⁰+Te1 EDF. However, there is no improvement in describing the peak energies systematically compared with those obtained using SGII EDFs with all the J^2 terms.

V. SUMMARY

In summary, we studied the GT transitions in four magic nuclei, ^{48}Ca , ^{90}Zr , ^{132}Sn and ^{208}Pb , using a self-consistent HF+SSRPA model with different Skyrme EDFs. The

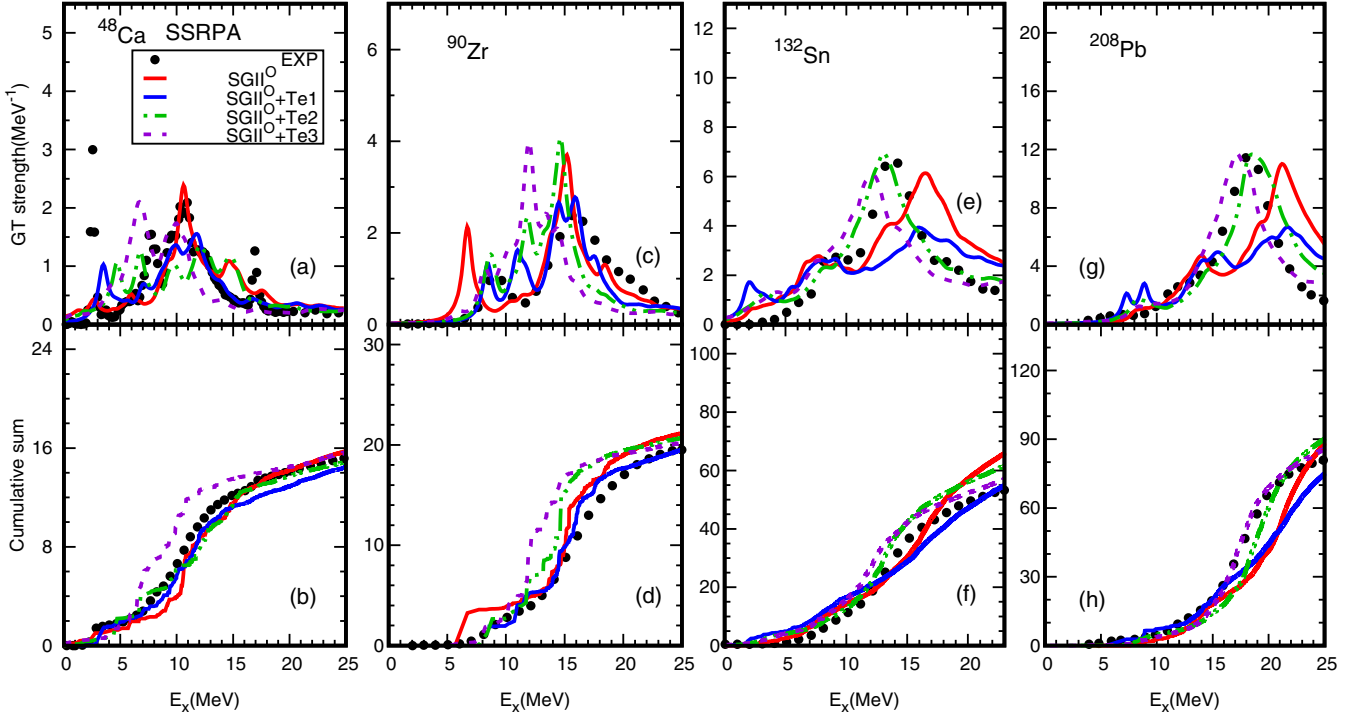


FIG. 9. Same as Fig. 8 but calculated without J^2 terms both in HF and SSRPA, and the results are labeled by SGII^{O} , $\text{SGII}^{\text{O}}+\text{Te1}$, $\text{SGII}^{\text{O}}+\text{Te2}$, and $\text{SGII}^{\text{O}}+\text{Te3}$, respectively.

SSRPA model describes systematically and quantitatively the GT strength distributions in the four nuclei better than the RPA model. Particularly the SGII and SAMi-T EDFs reproduce well the strength distributions of the main GT peaks in terms of the excitation energy and the peak height in comparison with the experimental data, except for ^{90}Zr , in which the calculated peak height is about a factor 2 larger than the experimental one. We examined the effect of tensor terms in the SAMi-T EDF and found that they shift the main peaks downwards by about 1 MeV in ^{48}Ca , ^{132}Sn , and ^{208}Pb , but have almost no effect in ^{90}Zr . The quenching factors are increased by about few percent, but these values with the tensor interactions are still about a half of the experimental quenching factors. We explored whether or not the tensor force with different strengths further increases the quenching factor of GT strength. To this end, we adopt the T21, T44, and T55 EDFs from the TIJ family with quite different values of the tensor terms. We realized that none of these three parameter sets provide a good description of the strength distributions, either in the excitation energies or in the peak heights. However, the T55 EDF produces large quenching factors: 30% for ^{48}Ca , 25% for ^{90}Zr , 27% for ^{132}Sn , and 19% for ^{208}Pb . In ^{208}Pb , the quenching factors are smaller, which may be related to the insufficient cutoff energy of 2p-2h configurations.

We studied further the role of tensor interactions on the quenching with the parameter sets $\text{SGII}+\text{Te1}$, $\text{SGII}+\text{Te2}$, and $\text{SGII}+\text{Te3}$, keeping the central part unchanged, but varying only the strength of the tensor interaction. With these parameter sets, we found that the tensor interactions affect

substantially the strength distributions of GT peaks; i.e., they have a strong effect on the spreading of the strength distribution and the shift of the excitation energy. Among the three different tensor parameters, $\text{SGII}+\text{Te1}$ reproduces at the best the GT strength distributions in the four nuclei as far as the excitation energy and the peak height are concerned. The $\text{SGII}+\text{Te1}$ and $\text{SGII}+\text{Te3}$ EDFs, in which the strengths of the triplet-odd tensor term are quite different even in the sign, produce large quenching factors similar to those of T55. In addition, as SGII is optimized excluding J^2 terms, we did the calculations in which the J^2 terms are excluded in both HF and SSRPA for the SGII EDF. The calculations show that the exclusion of J^2 terms of the momentum dependent interactions gives larger quenching factors, close to experimental data. However, the systematical description of the strength distributions in the four nuclei is not much improved compared to those with all the J^2 terms. It is still a future challenge to describe realistic strength distributions and the larger quenching factors with optimized Skyrme EDFs for the spin-isospin excitations including tensor terms.

ACKNOWLEDGMENTS

We are grateful to Di Wu for fruitful discussions. This work is supported by the National Natural Science Foundation of China under Grants No.11575120, and No. 11822504, by the Science Specialty Program of Sichuan University under Grant No. 2020SCUNL210, and by JSPS KAKENHI Grant No. JP19K03858.

- [1] M. N. Harakeh and A. van der Woude, *Giant Resonances: Fundamental High-Frequency Modes of Nuclear Excitation* (Oxford University Press, Oxford, 2001).
- [2] F. Osterfeld, *Rev. Mod. Phys.* **64**, 491 (1992).
- [3] M. Ichimura, H. Sakai, and T. Wakasa, *Prog. Part. Nucl. Phys.* **56**, 446 (2006).
- [4] T. Kajino, W. Aoki, A. B. Balantekin, R. Diehl, M. A. Famiano, and G. J. Mathews, *Prog. Part. Nucl. Phys.* **107**, 109 (2019).
- [5] F. T. Avignone, S. R. Elliott, and J. Engel, *Rev. Mod. Phys.* **80**, 481 (2008).
- [6] J. Engel and J. Menéndez, *Rep. Prog. Phys.* **80**, 046301 (2017).
- [7] D. J. Rowe, *Rev. Mod. Phys.* **40**, 153 (1968).
- [8] N. Auerbach, L. Zamick, and A. Klein, *Phys. Lett. B* **118**, 256 (1982).
- [9] T. H. R. Skyrme, *Nucl. Phys.* **9**, 615 (1958).
- [10] D. Vautherin and D. M. Brink, *Phys. Rev. C* **5**, 626 (1972).
- [11] M. Bender, J. Dobaczewski, J. Engel, and W. Nazarewicz, *Phys. Rev. C* **65**, 054322 (2002).
- [12] S. Fracasso and G. Colò, *Phys. Rev. C* **76**, 044307 (2007).
- [13] J. Decharge, M. Girod, and D. Gogny, *Phys. Lett. B* **55**, 361 (1975).
- [14] J. P. Blaizot and D. Gogny, *Nucl. Phys. A* **284**, 429 (1977).
- [15] J. Decharge and D. Gogny, *Phys. Rev. C* **21**, 1568 (1980).
- [16] N. Paar, T. Niksic, D. Vretenar, and P. Ring, *Phys. Rev. C* **69**, 054303 (2004).
- [17] H. Z. Liang, N. Van Giai, and J. Meng, *Phys. Rev. Lett.* **101**, 122502 (2008).
- [18] J. Meng, *Relativistic Density Functional for Nuclear Structure*, International Review of Nuclear Physics Vol. 10 (World Scientific, Singapore, 2016).
- [19] J. Speth and A. van der Woude, *Rep. Prog. Phys.* **44**, 719 (1981).
- [20] A. Van Der Woude, *Prog. Part. Nucl. Phys.* **18**, 217 (1987).
- [21] S. Ait-Tahar and D. Brink, *Nucl. Phys. A* **560**, 765 (1993).
- [22] S. Drożdż, S. Nishizaki, J. Speth, and J. Wambach, *Phys. Rep.* **197**, 1 (1990).
- [23] J. Rapaport, T. Taddeucci, T. P. Welch, C. Gaarde, J. Larsen, D. J. Horen, E. Sugarbaker, P. Koncz, C. C. Foster, C. D. Goodman, C. A. Goulding, and T. Masterson, *Nucl. Phys. A* **410**, 371 (1983).
- [24] Y. F. Niu, G. Colò, and E. Vigezzi, *Phys. Rev. C* **90**, 054328 (2014).
- [25] C. Robin and E. Litvinova, *Phys. Rev. Lett.* **123**, 202501 (2019).
- [26] D. Gambacurta, M. Grasso, and J. Engel, *Phys. Rev. Lett.* **125**, 212501 (2020).
- [27] D. Gambacurta and M. Grasso, *Phys. Rev. C* **105**, 014321 (2022).
- [28] A. Arima, K. Shimizu, W. Bentz, and H. Hyuga, in *Advances in Nuclear Physics*, edited by J. W. Negel and Erich W. Vogt (Springer, New York, 1988), Vol. 18, p. 1.
- [29] G. F. Bertsch and I. Hamamoto, *Phys. Rev. C* **26**, 1323 (1982).
- [30] C. L. Bai, H. Sagawa, H. Q. Zhang, X. Z. Zhang, G. Colò, and F. R. Xu, *Phys. Lett. B* **675**, 28 (2009).
- [31] C. L. Bai, H. Q. Zhang, X. Z. Zhang, F. R. Xu, H. Sagawa, and G. Colò, *Phys. Rev. C* **79**, 041301(R) (2009).
- [32] K. Ikeda, S. Fujita, and J. I. Fujita, *Phys. Lett.* **3**, 271 (1963).
- [33] D. Gambacurta, M. Grasso, and J. Engel, *Phys. Rev. C* **92**, 034302 (2015).
- [34] M. J. Yang, C. L. Bai, H. Sagawa, and H. Q. Zhang, *Phys. Rev. C* **103**, 054308 (2021).
- [35] N. Van Giai and H. Sagawa, *Phys. Lett. B* **106**, 379 (1981).
- [36] X. Roca-Maza, G. Colò, and H. Sagawa, *Phys. Rev. C* **86**, 031306(R) (2012).
- [37] S. H. Shen, G. Colò, and X. Roca-Maza, *Phys. Rev. C* **99**, 034322 (2019).
- [38] T. Lesinski, M. Bender, K. Bennaceur, T. Duguet, and J. Meyer, *Phys. Rev. C* **76**, 014312 (2007).
- [39] L.-G. Cao, S.-S. Zhang, and H. Sagawa, *Phys. Rev. C* **100**, 054324 (2019).
- [40] C. L. Bai, H. Q. Zhang, H. Sagawa, X. Z. Zhang, G. Colò, and F. R. Xu, *Phys. Rev. C* **83**, 054316 (2011).
- [41] K. Yako, M. Sasano, K. Miki, H. Sakai, M. Dozono, D. Frekers, M. B. Greenfield, K. Hatanaka, E. Ihara, M. Kato, T. Kawabata, H. Kuboki, Y. Maeda, H. Matsubara, K. Muto, S. Noji, H. Okamura, T. H. Okabe, S. Sakaguchi, Y. Sakemi *et al.*, *Phys. Rev. Lett.* **103**, 012503 (2009).
- [42] T. Wakasa, H. Sakai, H. Okamura, H. Otsu, S. Fujita, S. Ishida, N. Sakamoto, T. Uesaka, Y. Satou, M. B. Greenfield, and K. Hatanaka, *Phys. Rev. C* **55**, 2909 (1997).
- [43] J. Yasuda, M. Sasano, R. G. T. Zegers, H. Baba, D. Bazin, W. Chao, M. Dozono, N. Fukuda, N. Inabe, T. Isobe, G. Jhang, D. Kameda, M. Kaneko, K. Kisamori, M. Kobayashi, N. Kobayashi, T. Kobayashi, S. Koyama, Y. Kondo, A. J. Krasznahorkay *et al.*, *Phys. Rev. Lett.* **121**, 132501 (2018).
- [44] T. Wakasa, M. Okamoto, M. Dozono, K. Hatanaka, M. Ichimura, S. Kuroita, Y. Maeda, H. Miyasako, T. Noro, T. Saito, Y. Sakemi, T. Yabe, and K. Yako, *Phys. Rev. C* **85**, 064606 (2012).